Geological Society of America Bulletin

Proterozoic granites of the Llano Uplift, Texas: A collision–related suite containing rapakivi and topaz granites

Daniel S. Barker and Robert M. Reed

Geological Society of America Bulletin 2010;122;253-264
doi: 10.1130/B26451.1

Notes

Proterozoic granites of the Llano Uplift, Texas: A collision–related suite containing rapakivi and topaz granites

Daniel S. Barker[1,*] and Robert M. Reed[2]

[1]*Department of Geological Sciences, Jackson School of Geosciences, The University of Texas at Austin, 1 University Station C1100, Austin, Texas 78712-0254, USA*

[2]*Bureau of Economic Geology, Jackson School of Geosciences, The University of Texas at Austin, 1 University Station C1100, Austin, Texas 78712-0254, USA*

ABSTRACT

Proterozoic granites in the Llano Uplift, central Texas, intruded metamorphic rocks in a southern segment of the Grenville orogen. Three compositional groups of granite are present; two of these have not been previously recognized. The most widespread group occurs in three emplacement styles: (1) irregular plutons (synkinematic) were emplaced at 1119–1116 Ma during low-pressure Grenville metamorphism and deformation; (2) associated with these, there are volumetrically minor rhyolite dikes (1098–1093 Ma) and hypersolvus granite; and (3) large 1093–1072 Ma postkinematic circular to ovoid plutons are the most abundant of this compositional group, and many show rapakivi textures. A second, more felsic group has much higher light (L) to heavy (H) rare earth element (REE) ratios. The third group is highly fractionated, contains topaz locally, is enriched in Rb, Nb, and HREEs, and is depleted in Sr, Zr, and LREEs. No other igneous rocks were emplaced at the same time as the granites at the current level of exposure. Llano granites cannot be considered anorogenic or A-type on the basis of their tectonic setting, timing, or compositions. Sr, Nd, and Pb isotopic data indicate that these granites were derived from Proterozoic mantle and crust. The granites intruded thick continental crust at one margin of Laurentia and completed the consolidation of one segment of the Grenville orogen.

INTRODUCTION

According to the tectonic model of Mosher et al. (2008), southward subduction of a margin of Laurentia culminated (1150–1120 Ma) with collision of an arc (and obduction of an ophiolite), followed by continent-continent collision, crustal thickening, and uplift. From 1119 to 1116 Ma, and from 1098 to 1072 Ma, granite magma intruded, accompanied by slab detachment and upwelling of asthenospheric mantle.

Three lithotectonic domains (Mosher, 1998; Mosher et al., 2008) in the Llano Uplift make up the wall rocks for the granitic bodies (Fig. 1). These are the Valley Spring domain (1288–1232 Ma, probably part of the Midcontinent terrane of metamorphosed granite, rhyolite, and arkose protoliths), the Packsaddle domain (1274–1238 Ma, schists, marbles, and amphibolites probably derived from a forearc basin), and the Coal Creek domain (1326–1275 Ma, an accreted arc containing an ophiolite suite and gneissic tonalite-trondhjemite; Roback, 1996). The cited ages are U-Pb crystallization ages for igneous protoliths (Mosher, 1998). All three domains were juxtaposed before deformation, metamorphism, and the emplacement of the granites discussed in this paper.

Although much detailed work on geochronology, structural geology, and metamorphic petrology has recently been done in the Llano Uplift (summarized by Carlson et al., 2007; Mosher et al., 2008; Reed, 1999; Reese and Mosher, 2004), more complete characterization of the igneous rocks is necessary for better understanding of this strategic segment of Proterozoic crust (Fig. 1, inset). Metamorphic rocks of Grenville recrystallization age (1300–1000 Ma) extend to Oaxaca in southern Mexico, but no unmetamorphosed granites are known there (Ruiz et al., 1988; Cameron et al., 2004). Slightly more alkalic 1.12 Ga granites and syenites in the Franklin Mountains (west of El Paso) intruded undeformed sedimentary and volcanic rocks north of the Grenville Front (Smith et al., 1997; Li et al., 2006).

This paper presents petrographic descriptions, whole-rock major- and trace-element data, some mineral analyses, summaries of Sr, Nd, and Pb isotopic studies, and interpretations to further the knowledge of the Llano Uplift and its relations to other segments of the Grenville orogen, as well as the magmatic processes that operated in the area.

Pioneer workers in the Llano Uplift (summarized in Barnes et al., 1947) named five granitic lithostratigraphic units. Subsequent U-Pb geochronology (Walker, 1992; Helper et al., 1996; Roback et al., 1999; Reed, 1999; Rougvie et al., 1999; J.N. Connelly, 2006, personal commun.) on zircon and sphene (we prefer this name over titanite) contradicts this temporal sequence (Table 1), and the lithostratigraphic names will not be used in this paper.

Llano granites have been interpreted as A-type or anorogenic (Anderson, 1983) largely because of compositional similarities to Mesoproterozoic granites in the basement of west Texas and the Pikes Peak batholith of Colorado. However, Li et al. (2006, p. 69) concluded that "~1.1 Ga granite magmatism in the Llano region is difficult to classify according to granite type and tectonic setting." Furthermore, Smith et al. (1997, p. 70), in discussing their data on the postkinematic Enchanted Rock pluton in the Llano Uplift, stated that this pluton "exhibits features which overlap with granites emplaced in several tectonic settings" on such tectonic discrimination diagrams as Nb versus Y. Our data also provide evidence against an anorogenic setting and against an A-type compositional affinity.

Granitic intrusive rocks (Fig. 1) form ~42% of the Mesoproterozoic bedrock area exposed in the 9000 km^2 Llano Uplift of central Texas (Reed, 1999). These granites record major crustal events at one margin of Laurentia (Mosher, 1998; Reese and Mosher, 2004; Mosher et al., 2008). Sedimentary and igneous rocks older than ca. 1230 Ma in the Llano Uplift experienced high-pressure metamorphism at 775 °C and 2.5–1.7 GPa in the western part of the uplift, and 610–690 °C and 1.4 GPa in the north and east (Carlson et al., 2007). Most of the evidence for this and a somewhat later medium-pressure metamorphism (700 °C and 0.7 GPa) was obliterated when 1119–1072 Ma

*E-mail: danbarker@mail.utexas.edu

GSA Bulletin; January/February 2010; v. 122; no. 1/2; p. 253–264; doi: 10.1130/B26451.1; 7 figures; 3 tables; Data Repository item 2009136.

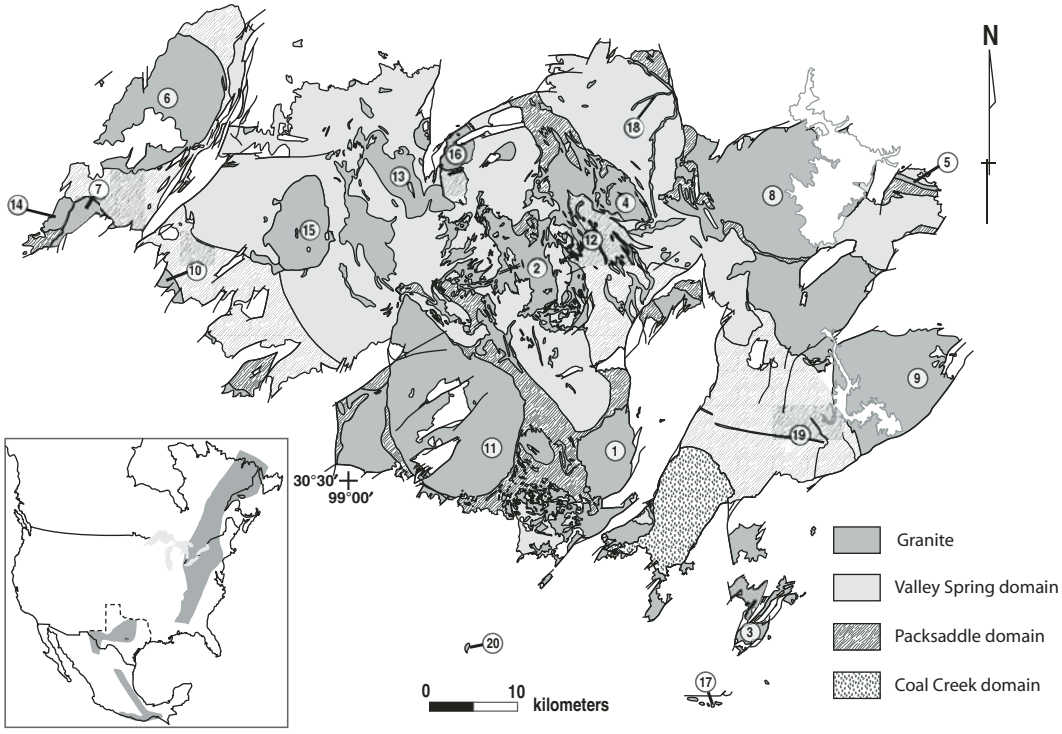

Figure 1. Geologic map of the Llano Uplift showing granite bodies and lithotectonic domains (after Reed, 1999). Numbers refer to granite bodies mentioned in this paper: 1—Legion Creek; 2—Sixmile; 3—Grape Creek; 4—Wolf Mountain; 5—Midway sill; 6—Katemcy; 7—Grit; 8—Lone Grove; 9—Granite Mountain; 10—Mason; 11—Enchanted Rock; 12—KC Quarry; 13—Kings Mountain; 14—Streeter; 15—Eckert; 16—Smoothingiron; 17—Morse Ranch; 18—porphyritic rhyolite dikes; 19—aphyric rhyolite dike; 20—Bear Mountain Quarry. Inset shows known extent of the Grenville orogen; the Llano Uplift is at the SE corner of the central Texas Grenville patch.

granite plutons were emplaced during an episode of lower-pressure metamorphism at 525–625 °C and 0.3 GPa (Carlson et al., 2007).

Recent petrologic studies have dealt with individual Llano plutons, and none has recognized the diversity of compositions. As late as 1996, Llano granites were thought to be one "remarkably homogeneous suite" (Barker et al., 1996), and one of our first aims was to test this supposition.

Two intrusive forms of granite are obvious on a generalized map (Fig. 1). One intrusive style produced irregular to sheetlike concordant bodies at 1119–1116 ± 6 Ma that were synkinematic. The other resulted in larger and postkinematic 1093–1072 ± 6 Ma plutons, roughly circular in plan, that show smooth discordant contacts. These contacts are vertical in the top few kilometers now preserved, according to drilling and gravity surveys (Muehlberger et al., 1963). The thicknesses of these plutons are not known, but if the scale-invariant postulate of McCaffrey and Petford (1997) is valid, they should have been 1.4–3.8 km thick before erosion, based on an average diameter of 10 km. Large roughly circular plutons occupy three or four times as much outcrop area as the smaller, more irregular bodies. Compositions of synkinematic and postkinematic granites and temporally intervening hypersolvus granite and rhyolite (Table 2) show only subtle differences. Two other granite groups form smaller bodies that intruded the larger granite bodies and metamorphic host rocks.

TABLE 1. U-Pb AGES (MA), LLANO GRANITES

Intrusion	Age (Ma)	Mineral	Reference
Synkinematic granites, irregular and sheetlike bodies			
Legion Creek pluton	1116 +6/–4	Zircon	Walker (1992)
Grape Creek pluton	1119 +6/–3	Zircon	Roback (1996, personal commun.)
Wolf Mtn pluton	1118 ± 5	Zircon	Reed (1999)
Wolf Mtn pluton	1116 ± 2	Sphene	Roback (1996, personal commun.)
Oatman Creek pluton	1119 ± 6	Sphene	Rougvie et al. (1999)
Rhyolitic dike rocks			
(porphyritic)	1093 ± 3	Zircon	Helper et al. (1996)
(aphyric)	1098 ± 3/–2	Zircon	Walker (1992)
Postkinematic granites, circular plutons			
Katemcy pluton	1070 ± 2	Zircon	Walker (1992)
Lone Grove pluton	1093 ± 6	Sphene	Rougvie et al. (1999)
Lone Grove pluton	1091 +4/–3	Zircon	Walker (1992)
Granite Mtn pluton	1091 ± 2	Zircon	Connelly (2006, personal commun.)
Enchanted Rock pluton	1080 ± 6	Zircon	Walker (1992)
High-Ce/Yb granites			
Wolf Mtn pluton	1117 ± 3	Zircon	Reed (1999)
Aplite dike	1076 ± 5	Sphene	Roback et al. (1999)
Topaz granites—no data (zircon metamict, sphene absent)			

METHODS

In the first phase of this study, 37 granite samples were analyzed in 1997 through 1999 by X-ray fluorescence (XRF) and inductively coupled plasma–mass spectrometry (ICP-MS) at one laboratory exclusively (Washington State University) in order to avoid interlaboratory variations. This sampling was not systematic, in that sites were not predetermined, and no more than five samples were analyzed from any one pluton. Most samples were from quarries and road cuts. Each sample was at least 2 kg, and coarser rock samples were 5 kg. Rocks were crushed using a steel roller and plate, and then an iron mortar, before taking an aliquot for powdering in a tungsten carbide mixer mill.

Major oxide component and some trace-element (V, Cr, Ni, Cu, Zn, Ga, and Zr) data are by XRF. ICP-MS data are for 14 rare earth elements plus Sc, Rb, Sr, Y, Nb, Cs, Ba, Hf, Ta, Pb, Th, and U. In addition to these 37, one sample of an aplite-pegmatite dike, one of an aphyric rhyolite dike, two of porphyritic rhyolite dikes, two of mafic schlieren in granites, and two of shear zones in granite were also analyzed by the Washington State University laboratory. Two analyses, 28 and 34, are replicates on the same

TABLE 2. MAJOR OXIDE AND TRACE-ELEMENT CONCENTRATIONS AND SELECTED RATIOS FOR LLANO GRANITES

	Synkinematic, irregular plutons *n* = 11		Hypersolvus granite and rhyolite dikes *n* = 4		Postkinematic, circular plutons *n* = 9		High Ce/Yb granites *n* = 5		Topaz granites *n* = 7	
	Avg	1σ	Avg	1σ	Avg	1σ	Avg	1σ	Avg	1σ
SiO_2 (wt%)	70.09	3.28	73.01	3.60	72.51	1.63	73.85	1.72	75.16	0.81
TiO_2	0.47	0.25	0.42	0.17	0.26	0.10	0.21	0.09	0.05	0.04
Al_2O_3	14.52	0.82	12.33	0.51	13.75	0.73	14.05	0.70	13.54	0.73
FeO*	3.13	1.20	3.82	2.38	2.30	0.73	1.63	0.48	1.24	0.20
MnO	0.06	0.03	0.07	0.05	0.04	0.02	0.02	0.01	0.04	0.04
MgO	0.93	0.57	0.19	0.09	0.20	0.13	0.38	0.15	0.07	0.11
CaO	1.73	0.70	0.92	0.69	1.17	0.31	1.14	0.27	0.61	0.18
Na_2O	3.63	0.35	3.24	0.50	3.53	0.45	3.17	0.25	4.28	0.69
K_2O	5.15	0.68	5.11	0.18	5.55	0.43	5.61	0.33	4.79	0.59
P_2O_5	0.14	0.09	0.08	0.05	0.07	0.03	0.07	0.04	0.03	0.05
Sc (ppm)	7.5	4.2	6.2	4.4	4.9	1.9	3.3	1.6	2.1	1.7
Ni	7	2	10	2	8	3	7	2	16	4
Zn	54	18	134	71	63	22	29	12	62	37
Ga	19	3	25	6	23	2	15	4	30	8
Rb	174	53	159	31	210	42	171	73	430	180
Sr	150	61	36	21	97	25	144	48	13	13
Y	65	20	143	42	83	26	14	4	131	46
Zr	314	116	742	344	305	116	173	73	118	36
Nb	17.0	3.4	42.7	10.5	18.5	5.0	6.2	2.2	44.4	19.9
Cs	3.2	2.2	2.9	4.3	3.5	2.5	3.1	1.8	6.7	4.9
Ba	841	333	434	224	624	240	739	298	64	64
La	61.7	20.9	108.0	22.3	65.9	29.5	57.2	25.9	18.1	17.5
Ce	120.2	38.5	224.6	45.4	134.0	59.7	106.4	49.7	46.5	38.0
Pr	13.5	4.2	26.9	5.2	15.7	6.9	10.8	5.1	5.7	5.4
Nd	52.6	15.3	110.6	24.4	62.0	26.3	38.2	18.0	24.9	23.4
Sm	11.6	3.4	25.8	6.3	14.3	5.8	6.4	2.4	9.2	7.2
Eu	1.78	0.75	2.33	0.90	1.64	0.47	1.04	0.23	0.28	0.27
Gd	10.6	3.3	24.1	7.0	12.9	4.9	4.03	0.98	11.1	7.1
Tb	1.79	0.58	4.11	1.20	2.27	0.84	0.52	0.10	2.47	1.36
Dy	11.2	3.7	25.3	7.5	14.3	5.1	2.61	0.41	17.8	7.9
Ho	2.30	0.76	5.25	1.55	2.92	1.01	0.49	0.10	4.22	1.46
Er	6.49	2.09	12.4	8.0	8.20	2.70	1.38	0.34	14.5	3.6
Tm	0.99	0.33	2.21	0.65	1.23	0.36	0.22	0.06	2.76	0.77
Yb	6.34	2.20	14.1	4.0	7.82	2.05	1.50	0.48	20.4	7.6
Lu	1.00	0.40	2.20	0.60	1.18	0.30	0.26	0.09	3.30	1.40
Hf	8.62	2.48	20.7	9.8	8.62	2.61	4.89	1.97	8.08	2.13
Ta	1.64	0.87	3.48	0.98	1.63	0.68	0.53	0.27	8.09	5.08
Pb	18.93	5.70	25.6	15.1	25.70	4.02	21.15	5.62	55.3	29.5
Th	18.52	9.00	12.00	3.70	15.80	6.19	17.29	4.20	29.3	9.7
U	3.92	2.77	3.62	1.65	3.55	1.25	2.88	1.02	10.4	7.0
Eu/Eu*	0.48	0.17	0.28	0.09	0.39	0.12	0.59	0.09	0.09	0.06
Ce_n/Yb_n	5.73	2.74	4.42	0.71	9.68	1.36	19.8	8.8	0.82	0.83
Rb/Sr	1.48	1.08	5.44	2.54	2.42	1.16	1.25	0.27	95.5	105.8
Rb/Ba	0.26	0.15	0.44	0.22	0.39	0.21	0.26	0.09	23.0	28.1
Zr/Nb	18.9	7.0	17.1	5.4	16.5	3.8	28.3	9.9	3.5	2.6
Zr/Hf	35.6	4.6	35.7	4.3	34.7	4.6	35.2	3.0	15.5	5.6
Nb/Ta	12.3	6.4	13.0	4.2	12.4	4.0	12.2	2.8	6.9	3.8
10^4 Sc/Al	2.53	0.29	3.85	0.79	3.14	0.26	2.93	0.45	4.25	0.88
Na/K	1.09	0.21	0.96	0.12	0.98	0.19	0.87	0.12	1.40	0.36
(Na + K)/Al	0.80	0.06	0.87	0.04	0.85	0.03	0.82	0.05	0.90	0.02
*T*zirc (°C)	832	30	924	42	829	31	793	41	748	13

Note: n—number of analyzed samples. Major oxide averages are normalized to 100%. All data are from the Washington State University Geoanalytical Laboratory. *T*zirc = zircon saturation temperature (Hanchar and Watson, 2003), calculated assuming that the whole-rock composition equals the liquid composition in equilibrium with zircon.

powder, analyzed in January 1998 and March 1999, respectively. They show very small differences, indicating highly reproducible analyses. Table DR-1 contains all 46 analyses, along with modal and other data.[1]

[1]GSA Data Repository item 2009136, containing 4 tables of whole-rock chemical and modal data for 46 samples, mineral compositions, and whole-rock Sm-Nd and Pb isotopic data, is available at http://www.geosociety.org/pubs/ft2009.htm or by request to editing@geosociety.org.

EMPLACEMENT STYLES AND COMPOSITIONAL GROUPS

In the nongenetic, nontectonic granite classification of Frost et al. (2001), the Llano granites are predominantly ferroan, alkali-calcic, and metaluminous. No sample qualifies as a leucogranite. All igneous rocks considered here are true granites according to their modal proportions of quartz, alkali feldspar, and plagioclase. Averaged major- and trace-element data are given in Table 2, and Table 3 summarizes mineralogical and textural variations. There are five columns in each of these tables because one compositional group displays three emplacement styles: synkinematic, postkinematic, and rhyolite dikes (hypersolvus granite is placed with the dikes because of similar composition). Emplacement styles of the other two compositional groups remain unclear, but they show irregular intrusive contacts against the first group. There are few significant variations in major-element proportions, but differences in mineralogy and in trace elements serve to discriminate the groups.

Rare earth element (REE) plots for 36 granite samples, normalized to average C1 chondrite values of Anders and Grevesse (1989), show differences among the granites (Fig. 2). These groups are distinguishable on grounds other than the REE proportions, as shown by Figure 3, which summarizes differences among trace-element concentrations and ratios.

TABLE 3. SUMMARY OF TEXTURAL AND MINERALOGICAL VARIATIONS AMONG GRANITES IN THE LLANO UPLIFT

Type/group	Synkinematic	Hypersolvus and rhyolite dikes	Postkinematic	High-Ce/Yb granite	Topaz granites
Schlieren	X	0	XX	0	0
Enclaves	XX	0	X	0	0
Mantled feldspars	X	0	X	0	0
Perthitic K-feldspar	XX	XX	X	X	XX
Zoned plagioclase	XX	0	XX	X	X
Myrmekite	XX	0	XX	X	0
Modes, vol% ± 1 standard deviation, at least 1000 points per thin section.					
Number of thin sections:	11	No modes	9	5	7
Quartz	30.3 ± 6.2	–	29.1 ± 8.7	31.1 ± 7.5	30.6 ± 5.1
K-feldspar	26.9 ± 10.3	–	34.3 ± 9.1	34.3 ± 3.3	34.8 ± 4.0
Plagioclase	23.0 ± 5.2	–	29.2 ± 13.7	26.0 ± 2.8	30.6 ± 3.2
Amphibole	1.2 ± 2.8	–	2.0 ± 2.5	0	0
Biotite	7.2 ± 3.9	–	4.6 ± 1.1	4.4 ± 2.8	2.0 ± 0.8
Muscovite	0	–	0	0.8 ± 0.2	0
Li mica	0	–	0	0	1.3 ± 1.0
Fluorite	Trace	–	Trace	Trace	0.4 ± 0.5
Sphene	0.6 ± 0.8	–	0.2 ± 0.2	Trace	0
Allanite	Trace	–	Trace	0.3 ± 0.2	0
Opaque oxides	0.3 ± 0.4	–	0.1 ± 0.1	0.1 ± 0.1	Trace
Others	0.6 ± 0.4	–	0.5 ± 0.3	0.3 ± 0.3	0.3 ± 0.3
Topaz	0	–	0	0	X
Monazite	0	–	Trace	XX	X
Xenotime	Trace	–	0	0	0
Thorianite	Trace	–	0	0	0
Zircon	X	–	X	X	Trace
Apatite	X	–	X	X	X
Garnet	0	–	0	0	Trace
Tourmaline	0	–	0	0	Trace
Rutile	X	–	X	X	X
Cassiterite	0	–	0	0	Trace
Barite	0	–	Trace	0	0
Galena	0	–	Trace	0	0
Columbite	0	–	0	0	Trace

Note: XX—common, X—rare, Trace—trace amounts in one or two thin sections, 0—not observed.

Synkinematic Granites

This type, the most numerous in the analyzed sample population but second in area exposed, was emplaced during the final stage of regional deformation (Reed, 1999), as indicated by weak foliations parallel to those in wall rocks and to axial planes of folds, the positions of some arcuate sheets of granite in hinges of folds, and the presence of deformed older dikes and undeformed younger ones from the same intrusive body invading wall rock. The Midway sill, emplaced along a southwest-dipping shear zone that brought Valley Spring over Packsaddle domain, was deformed into an augen gneiss. Similar shear occurred within the Grape Creek pluton. Mosher et al. (2004) provided additional structural evidence for intrusion during compressional deformation.

Hypersolvus Granite and Rhyolite Dikes

Only one analyzed granite sample (Table DR-1, #19 [see footnote 1]) is hypersolvus; all others contain discrete plagioclase outside alkali feldspar grains. Some of the rhyolites are aphyric (DeLong and Long, 1976) and others are porphyritic (Barker and Burmester, 1970). These rocks crop out over a much smaller total area than the synkinematic and postkinematic granites.

Postkinematic Plutons

The larger and younger plutons imposed static hydrothermal metamorphism on the wall rocks (Bebout and Carlson, 1986). Unoriented minerals (including sillimanite and cordierite) overgrew lineation and foliation in the metamorphic aureoles, indicating that most regional wall-rock deformation had ended by the time these larger granite plutons crystallized, although some deformation of wall rocks related to emplacement is present. Synkinematic and postkinematic plutons show the greatest spread in concentrations of most major-element oxide components (Table 2), reflecting variations in modal proportions. Granites of postkinematic plutons tend to be pink, coarse, and porphyritic like the synkinematic plutons. Postkinematic plutons typically show more abundant mafic schlieren and felsic enclaves than synkinematic bodies do, but fewer xenoliths; such features are not found in the two following groups.

The preceding three granite emplacement styles show one compositional cluster on variation diagrams (Fig. 3) and so will be considered as one compositional group, while the remaining two are distinct. The areal abundances of these two groups cannot be estimated, because of a lack of detailed mapping, but the total of these two must be less than 10% of the total for the first group.

High-Ce/Yb Granite

A second compositional group, more commonly gray than pink, finer and more equigranular, has the steepest negative slope ($Ce_n/Yb_n > 12$) on a chondrite-normalized rare earth diagram (Fig. 2); the subscript "n" denotes normalization to the chondrite values of Anders and Grevesse (1989). Uranium-lead ages from zircon and sphene (Table 1) are 1117 ± 3 and 1076 ± 5 Ma, approximately the same range as for the plutons and dikes of the first compositional group. High-Ce/Yb analyzed samples are from five separate bodies. In the few places where contacts are visible, this group forms irregular bodies that cut the first compositional group (the preceding three emplacement styles).

Topaz Granite

This granite, pink and equigranular to seriate, has the lowest Ce_n/Yb_n value (Fig. 2). There are no U-Pb ages for this group because zircons are sparse and metamict, and sphene is absent; dating of monazite has not yet been attempted. Other minerals include topaz, tourmaline, cassiterite, columbite, and Al-Li-F micas. The name "topaz granite" is used in place of more cumbersome labels, although topaz is no more an essential mineral in this granite than it is in the "topaz rhyolites" as defined by Christiansen et al. (1983). White (1960) described topaz-bearing pegmatites in the Streeter pluton and in other bodies of topaz granite. Analyzed samples of this group are from five widely separated bodies. The Llano topaz granites resemble the topaz-bearing granites associated with rapakivi granites in Finland (e.g., Haapala and Lukkari, 2004) in their high Rb and Ga, low Sr, Ba, Zr,

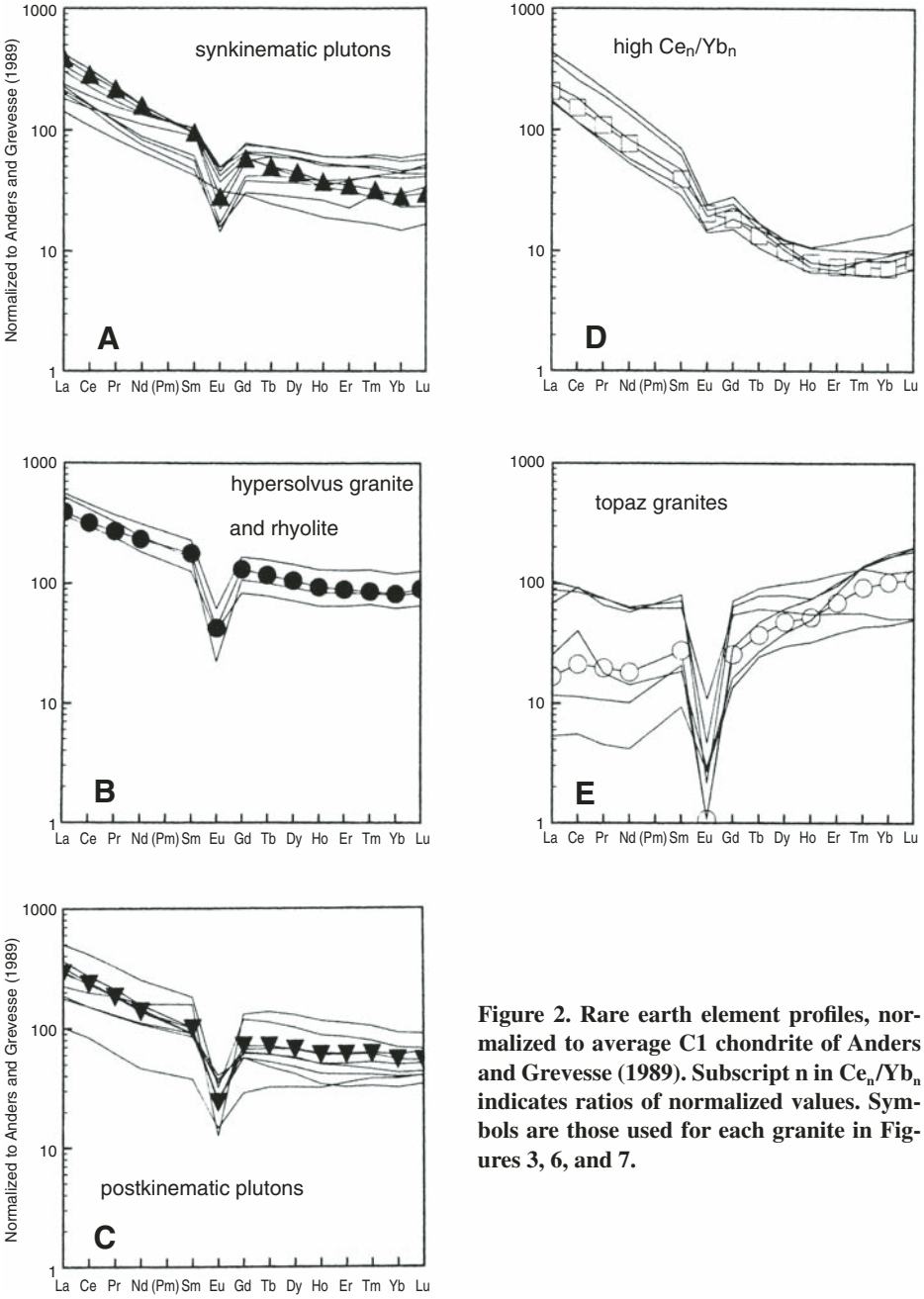

Figure 2. Rare earth element profiles, normalized to average C1 chondrite of Anders and Grevesse (1989). Subscript n in Ce_n/Yb_n indicates ratios of normalized values. Symbols are those used for each granite in Figures 3, 6, and 7.

and Zr/Hf, low Eu/Eu*, and the presence of Li-F micas, fluorite, monazite, and columbite.

To summarize chemical contrasts with the cluster representing the first compositional group, high-Ce/Yb granites have, in addition to the eponymous ratio, higher Sr and Ba, lower Y, Nb, Na, Zn, Ga, Hf, Ta, and U, and shallow Eu anomalies. The topaz granites, on the other hand, have lower ratios of light to heavy rare earth elements, lower Sr and Ba, lower Zr/Hf, higher Rb, Nb, Si, Na, Ni, Ga, Ta, Pb, Th, U, and (Na + K)/Al, and deep Eu anomalies. This group is lowest in Ti, Fe, Mg, Ca, K, P, Sc, and Zr.

The Grape Creek, Smoothingiron, and Eckert plutons contain topaz granite adjoining synkinematic and postkinematic granite. The Wolf Mountain pluton also contains representatives of two groups, and high-Ce/Yb cuts two pulses of synkinematic granite. The emplacement of granites of more than one type as successive small volumes within a pluton (Coleman et al., 2004) may reflect thermal control of magma emplacement rather than comagmatic derivation of the types. Later batches of ascending magma may preferentially follow routes within weaker and still hot igneous rock, or they may ascend along contacts between preceding batches and wall rock (Barker, 2007).

The synkinematic and postkinematic granites crop out over essentially the entire Llano Uplift in an area 100 km E-W and 60 km N-S. Synkinematic bodies, with few exceptions, occupy a NW-trending belt bracketed to the NE and SW by postkinematic plutons. Samples of high-Ce/Yb granite were found over an area centered in the north-central part of the uplift and with a 40-km-long WNW-trending axis and a 25-km-long SSW-trending axis. The area of topaz granite samples is nearly congruent with that of synkinematic and postkinematic granites and is 80 km E-W and 30 km N-S. Sparse occurrences of hypersolvus granite and rhyolite are found in a north-trending strip east of the center of the present exposure of Precambrian rocks.

Other Granites

Four samples, all from the active Bear Mountain quarry in the poorly exposed, undated, Hilltop pluton, do not conform to any of the other groups. Samples of this group are medium-grained, equigranular, and show obvious effects of subsolidus shear and recrystallization at lower temperatures than other Llano granites. The geographic isolation (10 km from the nearest outcrops of other granites) and aberrant composition of the Bear Mountain granite pose problems. Its extreme southern location indicates that this granite may have intruded the Coal Creek domain, although wall rock is not exposed; outcrops of the Bear Mountain granite are erosional remnants surrounded by onlapping Cretaceous sedimentary rocks south of the Llano Uplift. Although Table DR-1 (see footnote 1) includes whole-rock major- and trace-element data to aid future research, we offer no interpretation of the Bear Mountain granite.

TEXTURES AND INTERNAL STRUCTURES

Textural evidence generally supports data from mineralogy in the metamorphic aureoles that indicate the granite plutons were emplaced at ~10 km depth without rapid quenching (Reed, 1999; Reed and Rougvie, 2002). Pegmatites are common, and no miarolitic cavities have been seen.

In the synkinematic and postkinematic large plutons, K-feldspar megacrysts dominate. These are microcline microperthite, commonly showing Carlsbad twinning. The majority are rectangular in outline and vary from 1 to 5 cm in smallest dimension and 3–10 cm in largest dimension. Most are closely packed, in contact with other K-feldspar megacrysts. Some

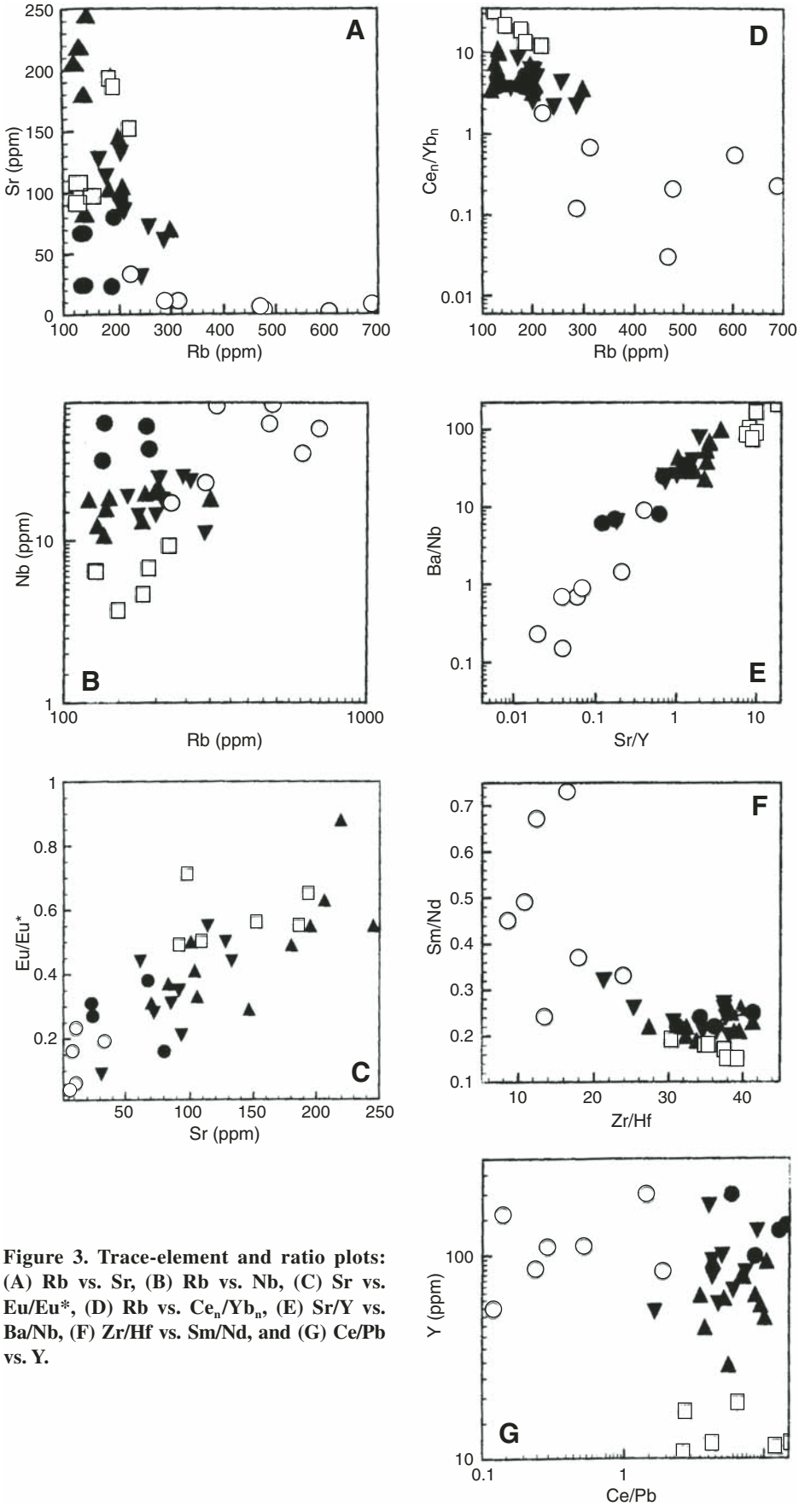

Figure 3. Trace-element and ratio plots: (A) Rb vs. Sr, (B) Rb vs. Nb, (C) Sr vs. Eu/Eu*, (D) Rb vs. Ce_n/Yb_n, (E) Sr/Y vs. Ba/Nb, (F) Zr/Hf vs. Sm/Nd, and (G) Ce/Pb vs. Y.

form larger radial aggregates of 5–8 crystals in which other minerals form <1 mm inclusions arranged concentrically and along boundaries between individual crystals of the feldspar aggregate (Fig. 4A). In high-Ce/Yb and topaz granites, alkali feldspar rarely exceeds 8 mm. Quartz and plagioclase are smaller than alkali feldspar in all groups. Plagioclase forms consistently smaller (3–8 mm), more equant crystals and aggregates, bordering, and enclosed by, the K-feldspar. Quartz is generally <3 mm, equant, anhedral, and interstitial to both K-feldspar and plagioclase in granites, and it forms euhedral bipyramidal phenocrysts in rhyolite dikes. Biotite and, where present, amphibole are interstitial to feldspars, and these two mafic minerals, with quartz, form linear arrays or chains between alkali feldspar crystals in some samples. These appear to have been swept aside by growing K-feldspar megacrysts.

Large Llano granite bodies locally show rapakivi texture (defined as perthitic microcline megacrysts rimmed by plagioclase; Ramo and Haapala, 1995). Rarely are more than 10% of the K-feldspar megacrysts in a sample mantled by plagioclase (~20 per m^2 as measured on polished slabs from the Granite Mountain quarry), and approximately three times as many plagioclase crystals have discrete K-feldspar rims. Some megacrysts of K-feldspar (~15 per m^2) have ovoid fine-grained equigranular cores, reaching 2 cm diameter, composed of quartz, plagioclase, K-feldspar, and biotite (Fig. 4B).

Some K-feldspar megacrysts (~15 per m^2) show concentric euhedral zoning emphasized by inclusions of plagioclase, amphibole, biotite, fluorite, and quartz. In the groundmass, accessory zircon, apatite, sphene, ilmenite, magnetite, and allanite are concentrated in or adjacent to amphibole and biotite.

Gently curving, steeply dipping schlieren containing more amphibole, biotite, sphene, and allanite, and locally with sparse K-feldspar crystals exceeding 10 cm, reach lengths of tens of meters and thicknesses of a few decimeters. Schlieren are common features in the postkinematic plutons. They are uncommon in synkinematic plutons and have not been seen in the other granites. Schlieren are concentrated near or at contacts between magma batches (where these can be inferred from differences in K-feldspar grain size, cores, or mantles), and they appear to have been segregated mechanically during subvertical movement of crystal-rich magma.

Fine equigranular enclaves have been found in postkinematic and synkinematic bodies, but they are not clearly associated with schlieren as are those documented by Wiebe et al. (2006). Enclaves have the same mineral assemblage as the enclosing granite. Silica contents of enclaves

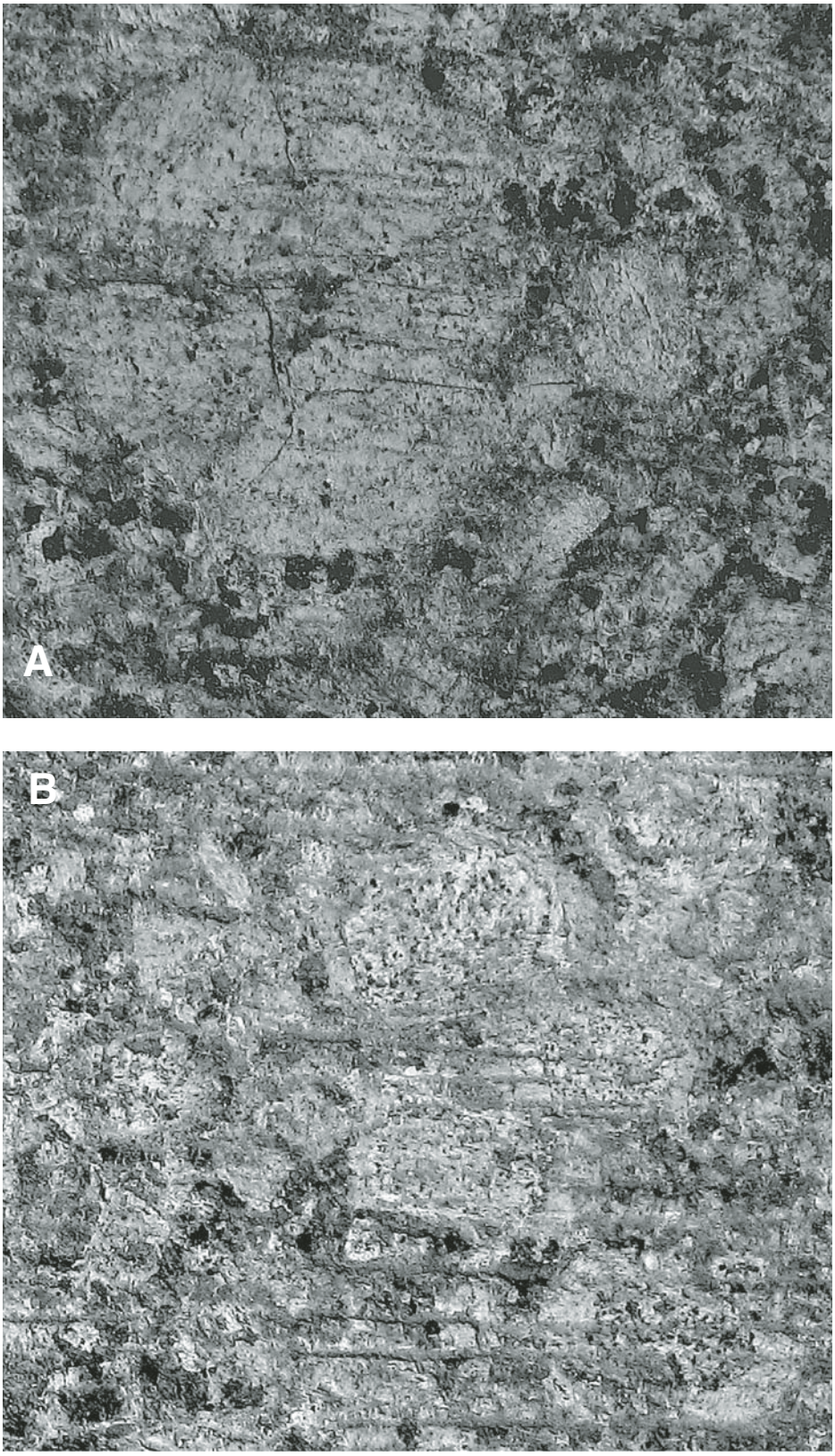

Figure 4. Photographs of sawed surfaces, postkinematic granite from Granite Mountain quarry. (A) Multiple megacryst of K-feldspar with concentric zones of mafic, plagioclase, and quartz inclusions. True scale. (B) Swarm of K-feldspars with fine equigranular cores, and dark plagioclase mantled by K-feldspar in lower left. True scale.

range from 66 to 70 wt%, and of the host granite range from 68.5 to 76.5 wt% at Enchanted Rock (Smith et al., 1997), and from 62.5 to 71.7 wt% and 66.5–77.0 wt % for enclaves and granite host, in the Granite Mountain pluton (Gallegos, 1995). The one analyzed enclave from the Wolf Mountain pluton has 64.7 wt% SiO_2, and its host has 68.3 wt% (Reed, 1999). Smith and Wark (1992) interpreted the enclaves at Enchanted Rock as chilled masses of slightly more mafic granite; enclaves have similar Pb and Nd isotopic ratios as the host granite (Smith et al., 1997).

MINERALOGY

Electron microprobe analyses were made by DSB in 1996–1999 using the JEOL 733 4-spectrometer probe in the Department of Geological Sciences, The University of Texas at Austin under operating conditions 15 kV, 20 nA, 2–30 µm spot diameters, 30 s counting times, ZAF data reduction; other analyses in 2004–2007 used the JEOL JXA-8200 5-spectrometer probe in the same department at 15 kV, 15 nA, 20 µm spot, 20 s, and ZAF. Average feldspar compositions and representative analyses for other minerals are provided in Table DR-2 (see footnote 1).

Accessory minerals (Table 3) were confirmed by energy-dispersive spectrometry after petrography and backscattered electron imaging. Three or four thin sections of each granite group were searched; therefore, some accessories were probably missed.

K-feldspar compositions ($An_{0–0.3}Ab_{3.2–7.3}Or_{93–97}$) show no significant variations among the granite groups, except for lower Ba in topaz granites. In postkinematic plutons, dark-gray plagioclase (An_{32} $Ab_{67}Or_1$) forms subhedral grains to 2 cm long (~15 per m^2). Aside from these, average plagioclase decreases in An content from synkinematic and postkinematic plutons ($An_{16}Ab_{83}Or_1$) through high-Ce/Yb granites ($An_{14}Ab_{85}Or_1$) to topaz granites ($An_3Ab_{96}Or_1$). All the feldspars are highly ordered, low-temperature forms as indicated by X-ray diffraction. In granites of synkinematic and postkinematic plutons, zones enriched in barium (<2 wt% BaO) occur in K-feldspar.

Amphibole was identified only in the synkinematic and postkinematic plutons, where pargasite and ferropargasite rim adjacent grains within a single thin section, and in hypersolvus granite. It coexists with quartz, K-feldspar, plagioclase, biotite, sphene, magnetite, and ilmenite and therefore seems to meet the minimum criteria for application of the aluminum-in-hornblende geobarometer (Johnson and Rutherford, 1989). However, microprobe analyses of amphibole within a single thin section

spanned a range of compositions and yielded estimated pressures of 0.3–0.4 GPa. Possible reasons for uncertainty are disequilibrium between amphibole and other phases, as indicated by the range in Mg/(Mg + Fe*) ratios of 0.38–0.65 in rims of amphibole within the same thin section, and possibly crystallization temperatures appreciably higher than the granite solidus (Anderson and Smith, 1995). The amphibole-plagioclase geothermometer of these authors was not used because it was uncertain which amphibole composition was equilibrated with which plagioclase, if any.

Micas are iron-rich biotites (Mg/[Mg + Fe*] = 0.12–0.33) in synkinematic and postkinematic plutons, and biotite and muscovite in high-Ce/Yb granites. Al-Li-F mica is restricted to topaz granites.

Sphene is abundant in the synkinematic and postkinematic plutons, less so in hypersolvus granite and rhyolite dikes, and rare or absent in high-Ce/Yb and topaz granite. Some is euhedral in quartz and K-feldspar, and some is in anhedral grains around ilmenite, between ilmenite and amphibole, and between biotite and plagioclase.

Ilmenite (X_{ilm} = 0.96) and magnetite (X_{usp} = 0.22) compositions in one synkinematic granite yielded estimates of 625 °C and oxygen fugacity close to the fayalite-magnetite-quartz buffer (Spencer and Lindsley, 1981). This temperature is reasonable for reactions below the granite solidus, and the oxygen fugacity falls on a trajectory shared by many intrusive granitic rocks (Spencer and Lindsley, 1981).

Zoned apatite, fluorite, and zircon are accessory minerals in all the granite groups. Apatite, as well as fluorite, shows concentric zoning in cathodoluminescence (CL) images, but, in contrast to zircon, in most samples, fluorite and apatite zoning is not truncated by resorption surfaces. In topaz granites, where it is especially common, fluorite has anhedral cores richer in Y than the rims. Our whole-rock data set does not include fluorine, although 16 analyses in Goldich (1941) and Barnes et al. (1947) report F from 0.02 to 0.25 wt%. Price et al. (1999) showed experimentally that, as fluorine content increases in a granitic liquid, amphibole gives way to biotite, and modal sphene diminishes as fluorite increases. Such a trend is shown by the Llano granites (Table 3), although this does not mean that the granites represent one continuous line of descent with increasing fluorine, for reasons discussed later herein.

Zircon is most common in, and adjacent to, biotite and amphibole, but it also occurs at quartz-quartz boundaries and within grains of quartz, K-feldspar, plagioclase, and sphene. Zircon provides much conflicting evidence concerning the magmatic history of the Llano granites and therefore is treated at length in a later section.

Allanite is a common accessory phase in high-Ce/Yb granites, occurs less commonly in synkinematic and postkinematic granites, and has not been identified in the topaz granites or hypersolvus granite. Much is metamict but retains concentric zoning.

Monazite is an uncommon accessory mineral, more commonly identified in the topaz and high-Ce/Yb granites. The enrichment in Th contrasting with depletion in Ce in the topaz granites and a lack of correlation between Ce and Th concentrations in the other groups suggest that monazite fractionation was not important (Montel, 1993). Nevertheless, we attribute the depletion in light rare earth elements in the topaz granite to removal of some of the observed monazite.

ZIRCON AND ITS MIXED MESSAGES

Zircon saturation temperatures (as formulated in Hanchar and Watson, 2003) are listed in Table DR-1 (see footnote 1). In all of these, the whole-rock analysis was assumed to represent the composition of magma (but see following for evidence against this assumption). In synkinematic and postkinematic granites, zircon temperatures average 832 ± 30 °C (1σ) and 829 ± 31 °C, respectively. Hypersolvus granite and rhyolites have zircon saturation temperatures of 924 ± 42 °C. For the high-Ce/Yb granites, the corresponding values are 793 ± 41 °C. Zircon temperatures for topaz granites are 748 ± 13 °C. Llano granites thus appear to show the dichotomy (Miller et al., 2003) between "hot granites" (>800 °C), and "cold granites" (<800 °C), but all Llano granite samples studied have inherited zircons that have gone through multiple episodes of growth and resorption, according to cathodoluminescence (CL) images discussed herein, and thus are not "hot" granites.

These zircon saturation temperatures are best regarded as second-order compositional parameters rather than actual magmatic temperatures, but they do emphasize differences between the topaz-bearing granites and the others. The gap is especially wide considering the interpretation (Miller et al., 2003) that the temperatures for "hot" granites are minimum estimates and those for "cold" granites are maxima.

CL images of zircons were generated by RMR in 2007, using an FEI XL30 scanning electron microscope equipped with an Oxford Instruments MonoCL detector. All imaging was done on in situ zircons in thin sections rather than zircon separates. Figure 5 reveals that the "hot granites" of the first compositional group contain zircons that show strikingly similar crystallization histories. Resorbed dark cores, 10–100 μm long, contain three or more surfaces that truncate zones. Cores are at least partially surrounded by resorbed bright overgrowths or replacements intercalated with or succeeded by dark zones that in turn are truncated by euhedral rims, which are commonly dark but in a few examples bright. The trace elements responsible for the zoning are unknown.

The high-Ce/Yb granites, which have "whole-rock" zircon saturation temperatures just below 800 °C, also have dark resorbed cores succeeded by discontinuous bright and dark overgrowths and dark euhedral rims. At least 10 truncation surfaces are visible in Figure 5G. The only "cold" granites, those bearing topaz, have sparse zircons that show fewer truncation surfaces, fewer bright patches and zones, and are most commonly metamict (Fig. 5H). These features suggest a less complicated history of long-term residence in an already highly fractionated liquid. The other granite groups in fact show the zircon zoning features expected (Miller et al., 2003) of "cold" granites, in contradiction to their calculated zircon saturation temperatures. Bea et al. (2007, p. 2332) also recognized this dilemma, attributing it to "disequilibrium processes that do not normally occur in granite magmas." We equate the disequilibrium process with open-system infiltration and expulsion of liquids of varying compositions through mush.

One source of uncertainty in zircon saturation temperatures is the assumption that a whole-rock analysis represents the liquid with which zircon was saturated. A simple calculation illustrates the uncertainty. Bachmann and Bergantz (2004) estimated that a maximum of 20% interstitial liquid in a crystal-rich mush could escape. If this liquid was a "haplogranite" (33% normative quartz, 34% albite, and 33% K-feldspar), it is possible to mix 20% of this liquid with 80% of a whole-rock analysis (the solid residuum) to calculate the temperature for a more felsic hypothetical mush before liquid escaped. In whole-rock analysis 24 in Table DR-1 (a synkinematic granite; see footnote 1) the calculated zircon saturation temperature is 786 °C at 161 ppm Zr. For want of no better data, we assume that the haplogranite liquid is removed at this same temperature. The liquid then has a calculated saturation zircon concentration of 244 ppm. The mix of 80% solid residuum and 20% liquid yields 178 ppm Zr and 796 °C for the mush before liquid escaped.

The compositional parameter M (= [Na + K + 2Ca]/[Al × Si] in cation fractions), used in calculating the saturation temperature, is 1.408 for the whole rock, 1.563 for the haplogranite liquid, and 1.439 for the initial mush. All three

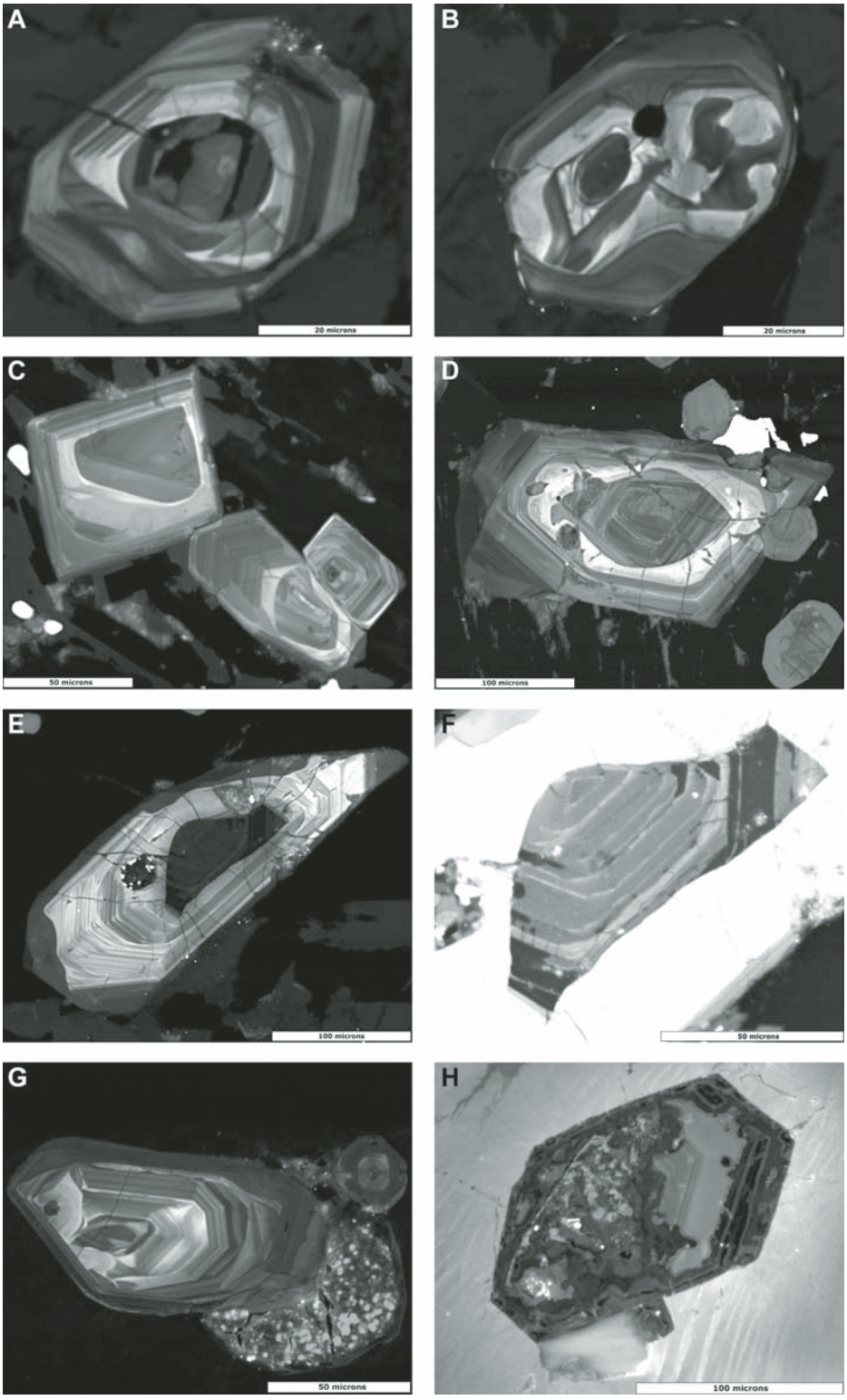

Figure 5. Scanning electron microscope (SEM)–based cathodoluminescence images of zircons showing complex zoning. (A) Synkinematic granite, GRLL-20. Note rounded core. (B) Same sample, with multiple cores. (C) Hypersolvus granite, GRLL-19. (D) Postkinematic granite GRLL-5. (E) Postkinematic granite, GRLL-5. Note dark core and dark euhedral overgrowth. (F) Enhanced-contrast image of core in 4E. (G) High-Ce/Yb granite, GRLL-28. (H) Topaz granite, GRLL-9. Note metamict core, partly resorbed light zone, and dark euhedral rim. Scale bars are 20 μm in A and B; 50 μm in C, F, and G; and 100 μm in D, E, and H.

changes (T, M, and ppm Zr) are relatively minor on the scale of Figure 6, suggesting that zircon saturation temperatures are actually quite robust.

A plot of zircon saturation temperatures versus whole-rock Zr content (Fig. 6) shows that the data define a narrow band having widths of 20–50 °C at constant Zr, 50–150 ppm Zr at constant temperature, and 0.4 M at constant temperature. Larger excursions in temperature, Zr, or M can explain the many dissolution and regrowth events shown in cathodoluminescence images as liquids varied between conditions of zircon saturation and undersaturation. Sufficient changes in temperature, Zr content, and M are likely to result from incursions of "new" magma and subsequent expulsion of fractionated interstitial liquid.

SUMMARY OF RELATIONS AMONG THE GRANITE GROUPS

We did not identify significant compositional trends within any of the groups, only differences between them. In postkinematic granites, the varied feldspar mantling attests to localized reaction between large feldspars and percolating liquid. So does the occurrence of amphibole, biotite, and quartz as zonally arranged inclusions in K-feldspar crystals and as interstitial clots and strands between them. Zonation of apatite and zircon and compositional variations in amphibole further demonstrate that crystallization occurred in liquids of locally differing compositions. Bachmann and Bergantz (2004) made a strong case for fractionated interstitial liquids migrating upward through crystal-rich (40%–50% solidified) mushes. Such liquids, interacting with crystals trapped in a mush, could efficiently account for the millimeter- to meter-scale inhomogeneities in the syn- and postkinematic granites. Lux et al. (2007) documented clear examples in the Deer Isle granite complex, Maine. Wark and Stimac (1992) envisioned the mantling of feldspars suspended in a largely liquid magma, but their mechanism of "rejuvenating" magma mingling with the in situ magma would work as well for hotter subjacent liquid percolating through crystal-rich mush. Whole-rock analyses of Llano synkinematic and postkinematic granites probably do not represent magma but crystal-rich residua after escape of unknown amounts of interstitial liquids that are not recognized at the exposed crustal level.

Because the K-feldspars in the postkinematic granites (Fig. 4A) are large, include other minerals that crystallized in liquid, and are zoned with respect to Ba, they have close similarities to those described by Moore and Sisson (2008). We follow their interpretation that the

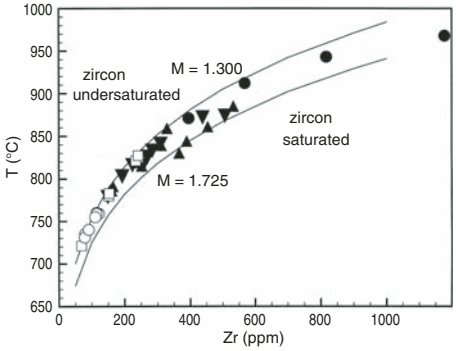

Figure 6. Plot of "whole-rock" zircon saturation temperatures vs. Zr (ppm). Two curves represent values of M = 1.30 and 1.725, where M = (Na + K + 2Ca)/(Al × Si) in cation proportions.

K-feldspar megacrysts grew slowly in liquid that was precipitating other minerals and that was episodically replenished. Furthermore, the K-feldspar megacrysts coexist, within spans of centimeters, with smaller K-feldspars mantled with plagioclase, plagioclase surrounded by K-feldspar, and K-feldspar cored by fine-grained aggregates of other minerals (Fig. 4B). This diversity reflects stirring of the mush during replenishment.

Upward migration of liquids through mushes in the large plutons cannot account for fractionation to produce the other granite groups at or near the exposed level. Zircon saturation temperatures are too high for hypersolvus granite and rhyolites to have fractionated from any other exposed group. Relative to synkinematic and postkinematic granites, topaz granites and high-Ce/Yb granites show contrasting enrichments and depletions (Fig. 3). Such divergence is difficult to reconcile with a single liquid line of descent, and it strongly suggests that these granite groups are not derived from one parent by a single process carried to different degrees. Least-squares major oxide modeling failed to reproduce either the high-Ce/Yb or topaz granites from the synkinematic and postkinematic granites. This is not surprising if, as already suggested, bulk compositions of the latter two represent mushes, not magmatic liquids.

In high-Ce/Yb granites, depletion in Y and in HREEs suggests a source containing residual garnet (but see following discussion under Magma Sources). Compositional contrasts with the topaz granites, for which there is strong evidence of fractionation, favor origin of the high-Ce/Yb granite magma by a contrasting mechanism. The homogeneity of analyzed samples of this group from small bodies over a large area does imply a deep and laterally widespread source.

In topaz granites, the low Sr contents (averaging 13 ppm) indicate that these highly evolved compositions were reached by extreme fractional crystallization, not by partial melting (cf. Halliday et al., 1991). Zr/Hf is less than 24 in topaz granites, but the ratio is higher in the other granites (Fig. 3F). Zr/Hf values lower than chondritic ratios (~30 and higher) are diagnostic of highly fractionated liquids separated from cumulates containing zircon (Claiborne et al., 2006). There is a rough correlation between low values of Eu/Eu* and Sr concentration (Fig. 3C). This is a further indication that topaz granites are the most highly fractionated (most depleted in Eu and Sr), and that feldspars were removed.

ISOTOPIC COMPOSITIONS

Published Sr, Nd, and Pb isotopic data are available for a few of the Llano granitic rocks (DeLong and Long, 1976; Garrison et al., 1979; Nelson and DePaolo, 1985; Patchett and Ruiz, 1989; Smith et al., 1997; Zartman, 1964, 1965). In general, published $^{87}Sr/^{86}Sr$ initial ratios in the granites are low (0.7034–0.7062) and ε_{Nd} values are high (+2.57 to +5.0). All indicate a significant mantle or "new" Proterozoic crustal component in the Llano granites. Both Sr and Nd isotopic data have not been published for the same Llano granite sample.

Roller (2004), under the supervision of J.N. Connelly, measured Sm, Nd, and Pb isotope abundances for some of the samples used for whole-rock major- and trace-element analyses in this paper. All Sm, Nd, and Pb isotope data, including those previously published, are available in Tables DR-3 and DR-4 (see footnote 1). The $(^{143}Nd/^{144}Nd)_t$, epsilon Nd_t, and T_{DM} values were all recalculated using revised age estimates. The epsilon Nd_t values are all positive (1.68–7.20), except for the synkinematic metamorphosed Midway sill (–0.65). The highest values, for topaz granites, reflect anomalously high Sm/Nd ratios shown by the rare earth profiles. The positive epsilon values for the other groups indicate that the granite sources were mantle and/or "young" mafic crust. The depleted mantle model ages (1.25 ± 0.10 Ga) for synkinematic and postkinematic granites, and for hypersolvus granite and rhyolite (1.25 ± 0.11 Ga), are all somewhat older than the emplacement ages of 1.08–1.12 Ga, favoring a source that was less than 200 Ma old at the time of granite emplacement. High-Ce/Yb granites have the highest T_{DM} values (1.32 ± 0.02 Ga); this could indicate an older source, but it more likely reflects differing proportions of mantle and crust contributions relative to the other granite groups.

The $^{207}Pb/^{204}Pb$ versus $^{206}Pb/^{204}Pb$ whole-rock data (Fig. 7) are best fit by a line with slope 0.083 ± 0.005, indicating derivation at 1.28 ± 0.12 Ga from a common lower crust or upper mantle source, the composition of which was estimated by James et al. (1994) to be $^{207}Pb/^{204}Pb$ = 15.37 and $^{206}Pb/^{204}Pb$ = 16.74. None of our isotopic or other data supports an Archean source for the Llano granites.

MAGMA SOURCES

Although mafic or intermediate magmas did not intrude to the same crustal level when the granites were emplaced, there are older gabbros, tonalities, and trondhjemites in the Llano Uplift (Roback, 1996), and some mantle-derived magma must have invaded or underplated newly accreted and thickened continental crust to provide heat to generate granite magmas (Huppert and Sparks, 1988). Underplated mafic rocks are one candidate for the granite magma source. Medium- to high-K basalts, typical of continental arc volcanism, are fertile sources for granitic magma (Sisson et al., 2005). Such intrusive rocks, or more likely their granulite or eclogite equivalents, could account for the low $^{87}Sr/^{86}Sr$ initial ratios and the moderately high εNd_t values of the Llano granites.

The level of the now-exposed erosion surface was intruded by granite magma when it was ~10 km deep at 1120–1070 Ma, but the wall rocks at that level of intrusion had been metamorphosed at ~20 km depth around 1150–1130 Ma, and possibly at more than 50 km depth before that (Carlson et al., 2007). Continental crust under the Llano Uplift is now ~40 km thick (Mooney and Braile, 1989). At the time of granite emplacement, it could have been at least 10 km thicker (erosion has removed 10 km). Although some migmatite did develop in the now-exposed Valley Spring Gneiss, there is no evidence that the granite plutons gathered their magmas from this exposed level. The granite sources were tens of kilometers deeper than the level of granite emplacement. Neither the estimated depth nor the isotopic data can discriminate between lower crust and mantle as sources.

It seems unlikely that any of the liquids giving rise to the Llano granites separated from their sources with the same composition that the granites now have. During tens of kilometers of ascent, magma must have partially crystallized, in conduits if not in crustal reservoirs. Llano topaz granites approach, but do not fall in, the compositional field of peraluminous leucogranites, which are thought to be the only granites produced exclusively by crustal melting (Patino Douce, 1999). However, the low Sr contents and Zr/Hf ratios of the topaz granites

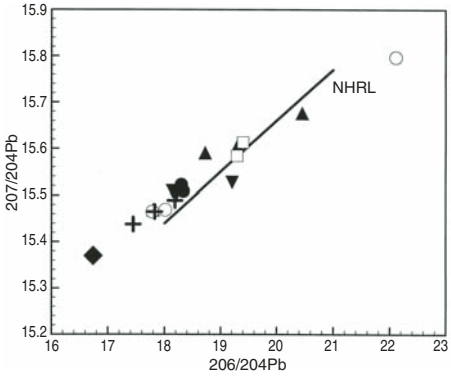

Figure 7. $^{206}Pb/^{204}Pb$ vs. $^{207}Pb/^{204}Pb$ (data from Table DR-4 [see footnote 1]). Enchanted Rock data (Smith et al., 1997) are shown by three plus signs. Black diamond represents estimate of lower crust or upper mantle source by James et al. (1994). NHRL—Northern Hemisphere reference line from Hart (1984).

indicate extreme fractionation, not a small degree of melting.

The observation that synkinematic granites (1119–1116 Ma), hypersolvus granite and rhyolite (1098–1093 Ma), and postkinematic granites (1093–1072 Ma) have the same bulk composition indicates, as do their identical depleted mantle model ages, that not only did these three emplacement types originate from similar sources, but they showed no significant depletion in granitic components over ~50 Ma. Partial melting of different volumes of the sources, prompted by injections of mafic magma at different times (Annen et al., 2006), is our preferred explanation for generation of magmas parental to the granites.

The high-Ce/Yb granites have light to heavy rare earth element ratios and depletion in Y that suggest that the source differed from those of the other granites in containing garnet, which retains Y and the heavy rare earth elements in the unmelted residue. Bachmann et al. (2005) showed that fractionation of amphibole and sphene can deplete Y and the heavy rare earth elements in granitic liquid to the same extent as garnet. A lack of upward concavity in rare earth patterns combined with the absence of amphibole support the role of garnet as a residual phase in generation of high-Ce/Yb granites. The topaz granites are products of fractionation of an unknown parental magma. The Pb isotope data, however, indicate a magma source similar to that of the other Llano granites. At present, it is impossible to estimate the relative contributions of mantle and crust to these sources, although both seem to have been involved.

CONCLUSIONS

The Llano granites investigated in this study were emplaced during and after low-pressure Grenville metamorphism from magmas generated in lower continental crust that was less than 200 Ma older. The large plutons are remnants of crystal mushes, heterogeneous on a scale of tens of centimeters, through which granitic liquid percolated. The rhyolite and hypersolvus, high-Ce/Yb, and topaz granites more closely approximate magmatic liquid compositions. The Llano granites are products of large-volume vertical migration of melts in continental crust at the southern margin of Laurentia, and they intruded three tectonic domains after accretion. They are synkinematic and postkinematic, not anorogenic or A-type, and they differ from other Proterozoic granites in Texas in their compositions and host rocks. The synkinematic granites began to intrude while compressional deformation was still going on, and possibly before slab detachment.

ACKNOWLEDGMENTS

We thank Jim Connelly, Liz Roller, and Bob Roback for allowing us to use their unpublished isotope data, and Bernard Bonin, Bill Carlson, Steve Clabaugh, Charles Gilbert, Mark Helper, Leon Long, Fred McDowell, Sharon Mosher, Bill Muehlberger, Tapani Ramo, Bob Roback, Jim Rougvie, Diane Smith, Doug Smith, Nick Walker, and the late Virgil Barnes for conversations that broadened and corrected our ideas. Calvin Miller, Guilherme Gualda, and Bernard Bonin provided constructive and detailed reviews. At the Washington State University Geoanalytical Laboratory, Diane Johnson and Charles Knaack delivered superior and timely data. This research was supported by the Geology Foundation of the Jackson School of Geosciences, The University of Texas at Austin.

REFERENCES CITED

Anders, E., and Grevesse, N., 1989, Abundances of the elements: Meteoritic and solar: Geochimica et Cosmochimica Acta, v. 53, p. 197–214, doi: 10.1016/0016-7037(89)90286-X.

Anderson, J.L., 1983, Proterozoic anorogenic granite plutonism of North America, *in* Medaris, L.G., Jr., Byers, C.W., Mickelson, D.M., and Shanks, W.C., eds., Proterozoic geology: Selected papers from an international Proterozoic symposium: Geological Society of America Memoir 161, p. 133–154.

Anderson, J.L., and Smith, D.R., 1995, The effects of temperature and oxygen fugacity on the Al-in-hornblende barometer: The American Mineralogist, v. 80, p. 549–559.

Annen, C., Scaillet, B., and Sparks, R.S.J., 2006, Thermal constraints on the emplacement rate of a large intrusive complex: The Manaslu leucogranite, Nepal, Himalaya: Journal of Petrology, v. 47, p. 71–95, doi: 10.1093/petrology/egi068.

Bachmann, O., and Bergantz, G.W., 2004, On the origin of crystal-poor rhyolites extracted from batholithic crystal mushes: Journal of Petrology, v. 45, p. 1565–1582, doi: 10.1093/petrology/egh019.

Bachmann, O., Dungan, M.A., and Bussy, F., 2005, Insights into shallow magmatic processes in large silicic magma bodies: The trace element record of the Fish Canyon magma body, Colorado: Contributions to Mineralogy and Petrology, v. 149, p. 338–349, doi: 10.1007/s00410-005-0653-z.

Barker, D.S., 2007, Endogenous and exogenous plutons: The influence of emplacement style on contamination of granitic magma: Canadian Mineralogist, v. 45, p. 63–70, doi: 10.2113/gscanmin.45.1.63.

Barker, D.S., and Burmester, R.F., 1970, Leaching of quartz from Precambrian hypabyssal rhyolite porphyry, Llano County, Texas: Contributions to Mineralogy and Petrology, v. 28, p. 1–8, doi: 10.1007/BF00389222.

Barker, D.S., Muehlberger, W.R., and Reed, R.M., 1996, Stop 12: Coarse-grained granite at Wirtz Dam, *in* Mosher, S., ed., Guide to the Precambrian Geology of the Eastern Llano Uplift, Central Texas: Field Trip Guide for the Geological Society of America 30th Annual South-Central Section Meeting: Austin, University of Texas at Austin, p. 33–40.

Barnes, V.E., Dawson, R.F., and Parkinson, G.A., 1947, Building Stones of Central Texas: University of Texas Publication 4246, 198 p.

Bea, F., Montero, P., Gonzalez-Lodeiro, F., and Talavera, C., 2007, Zircon inheritance reveals exceptionally fast crustal magma generation processes in central Iberia during the Cambro-Ordovician: Journal of Petrology, v. 48, p. 2327–2339, doi: 10.1093/petrology/egm061.

Bebout, G.E., and Carlson, W.D., 1986, Fluid evolution and transport during metamorphism: Evidence from the Llano Uplift, Texas: Contributions to Mineralogy and Petrology, v. 92, p. 518–529, doi: 10.1007/BF00374433.

Cameron, K.L., Lopez, R., Ortega-Gutierrez, F., Solori, L., Keppie, J.D., and Schulze, C., 2004, U-Pb geochronology and Pb isotopic compositions of leached feldspars: Constraints on the origin and evolution of Grenville rocks from eastern and southern Mexico, Tollo, R.P., McLelland, J., Corriveau, L., and Bartholemew, M.J., eds., Proterozoic tectonic evolution of the Grenville orogen in North America: Geological Society of America Memoir 197, p. 755–760.

Carlson, W.D., Anderson, S.D., Mosher, S., Davidow, J.S., Crawford, W.D., and Lane, E.D., 2007, High-pressure metamorphism in the Texas Grenville orogen: Mesoproterozoic subduction of the southern Laurentian continental margin: International Geology Review, v. 49, p. 99–119, doi: 10.2747/0020-6814.49.2.99.

Christiansen, E.H., Burt, D.M., Sheridan, M.F., and Wilson, R.T., 1983, Petrogenesis of topaz rhyolites from the western United States: Contributions to Mineralogy and Petrology, v. 83, p. 16–30.

Claiborne, L., Miller, C.F., Walker, B.A., Wooden, J.L., Mazdab, F.K. and Bea, F., 2006, Tracking magmatic processes through Zr/Hf ratios in rocks and Hf and Ti zoning in zircons: An example from the Spirit Mountain batholith, Nevada: Mineralogical Magazine, v. 70, p. 517–543.

Coleman, D.S., Gray, W., and Glazner, A.F., 2004, Rethinking the emplacement and evolution of zoned plutons: Geochronological evidence for incremental assembly of the Tuolumne Intrusive Suite, California: Geology, v. 32, p. 433–436, doi: 10.1130/G20220.1.

DeLong, S.E., and Long, L.E., 1976, Petrology and Rb-Sr age of Precambrian rhyolitic dikes, Llano County, Texas: Geological Society of America Bulletin, v. 87, p. 275–280, doi: 10.1130/0016-7606(1976)87<275:PARAOP>2.0.CO;2.

Frost, B.R., Barnes, C.G., Collins, W.J., Arculus, R.J., Ellis, D.J., and Frost, C.D., 2001, A geochemical classification for granitic rocks: Journal of Petrology, v. 42, p. 2033–2048, doi: 10.1093/petrology/42.11.2033.

Gallegos, M.A., 1995, Petrology and Geochemistry of the 1.05–1.06 Ga Marble Falls Intrusive Center, Llano Uplift, Central Texas [M.S. thesis]: San Antonio, University of Texas at San Antonio, 121 p.

Garrison, J.R., Jr., Long, L.E., and Richmann, D.L., 1979, Rb-Sr and K-Ar geochronologic and isotopic studies, Llano Uplift, central Texas: Contributions to Mineralogy and Petrology, v. 69, p. 361–374, doi: 10.1007/BF00372262.

Goldich, S.S., 1941, Evolution of the central Texas granites: The Journal of Geology, v. 49, p. 697–720.

Haapala, I., and Lukkari, S., 2005, Petrological and geochemical evolution of the Kymi stock, a topaz

granite cupola within the Wiborg rapakivi batholith, Finland: Lithos, v. 80, p. 347–362, doi: 10.1016/j.lithos.2004.05.012.

Halliday, A.N., Davidson, J.P., Hildreth, W., and Holden, P., 1991, Modelling the petrogenesis of high Rb/Sr silicic magmas: Chemical Geology, v. 92, p. 107–114, doi: 10.1016/0009-2541(91)90051-R.

Hanchar, J.M., and Watson, E.B., 2003, Zircon saturation thermometry, *in* Hanchar, J.M., and Hoskin, P.W.O., eds., Zircon: Reviews in Mineralogy and Geochemistry, v. 53, p. 89–112.

Hart, S.R., 1984, The Dupal anomaly: A large-scale isotope anomaly in the Southern Hemisphere mantle: Nature, v. 309, p. 753–757, doi: 10.1038/309753a0.

Helper, M.A., Gose, W.A., and Roback, R.C., 1996, Virtual geomagnetic pole positions from 1.1 Ga intrusive rocks of the Llano Uplift, central Texas: Geological Society of America Abstracts with Programs, v. 28, no. 1, p. 18.

Huppert, H.E., and Sparks, R.S.J., 1988, The generation of granitic magmas by intrusion of basalt into continental crust: Journal of Petrology, v. 29, p. 599–624.

James, E.W., Henry, C.D., and McDowell, F.W., 1994, Defining the southeastern limit of North American middle Proterozoic basement in Texas and Chihuahua with lead isotopes: Geological Society of America Abstracts with Programs, v. 26, no. 6, p. A20.

Johnson, M.C., and Rutherford, M.J., 1989, Experimental calibration of the aluminum-in-hornblende geobarometer with application to Long Valley caldera (California) volcanic rocks: Geology, v. 17, p. 837–841, doi: 10.1130/0091-7613(1989)017<0837:ECOTAI>2.3.CO;2.

Li, Y., Barnes, M.A., Barnes, C.G., and Frost, C.D., 2007, Grenville-age A-type and related magmatism in southern Laurentia, Texas and New Mexico, USA: Lithos, v. 97, p. 58–87, doi: 10.1016/j.lithos.2006.12.010.

Lux, D.R., Hooks, B., Gibson, D., and Hogan, J.P., 2007, Magma interactions in the Deer Isle granite complex, Maine: Field and textural evidence: Canadian Mineralogist, v. 45, p. 131–146, doi: 10.2113/gscanmin.45.1.131.

McCaffrey, K.J.W., and Petford, N., 1997, Are granitic intrusions scale invariant?: Journal of the Geological Society, v. 154, p. 1–4, doi: 10.1144/gsjgs.154.1.0001.

Miller, C.F., McDowell, S.M., and Mapes, R.W., 2003, Hot and cold granites? Implications of zircon saturation temperatures and preservation of inheritance: Geology, v. 31, p. 529–532.

Montel, J.-M., 1993, A model for monazite/melt equilibrium and application to the generation of granitic magmas: Chemical Geology, v. 110, p. 127–146, doi: 10.1016/0009-2541(93)90250-M.

Mooney, W.D., and Braile, L.W., 1989, The seismic structure of the continental crust and upper mantle of North America, *in* Bally, A.W., and Palmer, A.R., eds., The Geology of North America—An overview: Boulder, Colorado, Geological Society of America, The Geology of North America, v. A, p. 39–52.

Moore, J.G., and Sisson, T.W., 2008, Igneous phenocrystic origin of K-feldspar megacrysts in granitic rocks from the Sierra Nevada batholith: Geosphere, v. 4, p. 387–400, doi: 10.1130/GES00146.1.

Mosher, S., 1998, Tectonic evolution of the southern Laurentian Grenville orogenic belt: Geological Society of America Bulletin, v. 110, p. 1357–1375, doi: 10.1130/0016-7606(1998)110<1357:TEOTSL>2.3.CO;2.

Mosher, S., Hoh, A.M., Zumbro, J., and Reese, J.F., 2004, Tectonic evolution of the eastern Llano Uplift, central Texas: A record of Grenville orogenesis along the southern Laurentian margin, *in* Tollo, R.P., McLelland, J., Corriveau, L., and Bartholemew, M.J., eds., Proterozoic tectonic evolution of the Grenville orogen in North America: Geological Society of America Memoir 197, p. 783–798.

Mosher, S., Levine, J.S.F., and Carlson, W.D., 2008, Mesoproterozoic plate tectonics: A collisional model for the Grenville-aged orogenic belt in the Llano Uplift, central Texas: Geology, v. 36, p. 55–58, doi: 10.1130/G24049A.1.

Muehlberger, W.R., Bhatrakarn, T., and Youash, Y.Y., 1963, Correlation of geology and gravity observations in southern Burnet County, Texas: The Texas Journal of Science, v. 15, p. 35–49.

Nelson, B.K., and DePaolo, D.J., 1985, Rapid production of continental crust 1.7 to 1.9 b.y. ago: Nd isotopic evidence from the basement of the North American midcontinent: Geological Society of America Bulletin, v. 96, p. 746–754, doi: 10.1130/0016-7606(1985)96<746:RPOCCT>2.0.CO;2.

Patchett, P.J., and Ruiz, J., 1989, Nd isotopes and the origin of Grenville-age rocks in Texas: Implications for Proterozoic evolution of the United States Mid-continent region: The Journal of Geology, v. 97, p. 685–695.

Patino Douce, A.E., 1999, What do experiments tell us about the relative contributions of crust and mantle to the origin of granitic magmas?, *in* Castro, A., Hernandez, C., and Vigneresse, J.L., eds., Understanding granites: Integrating new and classical techniques: Geological Society of London Special Publication 168, p. 55–75, doi: 10.1144/GSL.SP.1999.168.01.05.

Price, J.D., Hogan, J.P., Gilbert, M.C., London, D., and Morgan, G.B.V.I., 1999, Experimental study of titanite-fluorite equilibria in the A-type Mount Scott Granite: Implications for assessing F contents of felsic magma: Geology, v. 27, p. 951–954, doi: 10.1130/0091-7613(1999)027<0951:ESOTFE>2.3.CO;2.

Ramo, O.T., and Haapala, I., 1995, One hundred years of Rapakivi Granite: Mineralogy and Petrology, v. 52, p. 129–185, doi: 10.1007/BF01163243.

Reed, R.M., 1999, Emplacement and Deformation of Late Syn-Orogenic, Grenville-Age Granites in the Llano Uplift, Central Texas [Ph.D. thesis]: Austin, The University of Texas at Austin, 271 p.

Reed, R.M., and Rougvie, J.R., 2002, Low-pressure deformation and metamorphism of the Proterozoic Llano Uplift, central Texas: Geological Society of America Abstracts with Programs, v. 34, no. 3, p. A7.

Reese, J.F., and Mosher, S., 2004, Kinematic constraints on Rodinia reconstructions from the core of the Texas Grenville orogen: The Journal of Geology, v. 112, p. 185–205, doi: 10.1086/381657.

Roback, R.C., 1996, Characterization and tectonic evolution of a Mesoproterozoic island arc in the southern Grenville orogen, Llano Uplift, central Texas: Tectonophysics, v. 265, p. 29–52, doi: 10.1016/S0040-1951(96)00145-X.

Roback, R.C., Hunt, B.B., and Helper, M.A., 1999, Mesoproterozoic tectonic evolution of the western Llano Uplift, central Texas: The story in an outcrop: Rocky Mountain Geology, v. 34, p. 275–287, doi: 10.2113/34.2.275.

Roller, E.A., 2004, Petrogenesis of the Llano Granites, Central Texas: Formation Mechanisms and Tectonic Implications of Radiogenic Isotopes [M.S. thesis]: Austin, The University of Texas at Austin, 116 p.

Rougvie, J.R., Carlson, W.D., Copeland, P., and Connelly, J.N., 1999, Late thermal evolution of Proterozoic rocks in the northeastern Llano Uplift, central Texas: Precambrian Research, v. 94, p. 49–72, doi: 10.1016/S0301-9268(98)00103-X.

Ruiz, J., Patchett, P.J., and Ortega-Gutierrez, F., 1988, Proterozoic and Phanerozoic basement terranes of Mexico from Nd isotopic studies: Geological Society of America Bulletin, v. 100, p. 274–281, doi: 10.1130/0016-7606(1988)100<0274:PAPBTO>2.3.CO;2.

Sisson, T., Ratajeski, K., Hankins, W.B., and Glazner, A.F., 2005, Voluminous granitic magmas from common basaltic sources: Contributions to Mineralogy and Petrology, v. 148, p. 635–661, doi: 10.1007/s00410-004-0632-9.

Smith, D.R., and Wark, D.A., 1992, Magmatic enclaves in the Enchanted Rock batholith, Llano Uplift, Texas: Geological Society of America Abstracts with Programs, v. 24, no. 1, p. A47.

Smith, D.R., Barnes, C., Shannon, W., Roback, R., and James, E., 1997, Petrogenesis of Mid-Proterozoic granitic magmas: Examples from central and west Texas: Precambrian Research, v. 85, p. 53–79, doi: 10.1016/S0301-9268(97)00032-6.

Spencer, K.J., and Lindsley, D.H., 1981, A solution model for coexisting iron-titanium oxides: The American Mineralogist, v. 66, p. 1189–1201.

Walker, N.W., 1992, Middle Proterozoic geologic evolution of the Llano Uplift, Texas: Evidence from U-Pb zircon geochronometry: Geological Society of America Bulletin, v. 104, p. 494–504, doi: 10.1130/0016-7606(1992)104<0494:MPGEOL>2.3.CO;2.

Wark, D.A., and Stimac, J.A., 1992, Origin of mantled (rapakivi) feldspars: Experimental evidence of a dissolution- and diffusion-controlled mechanism: Contributions to Mineralogy and Petrology, v. 111, p. 345–361, doi: 10.1007/BF00311196.

White, J.W., 1960, Topaz-Bearing Pegmatites and Gem Topaz in the Llano Uplift, Texas [M.A. thesis]: Austin, University of Texas, 95 p.

Wiebe, R.A., Jellinek, M., Markley, M.J., Hawkins, D.P., and Snyder, D., 2007, Steep schlieren and associated enclaves in the Vinalhaven granite, Maine: Possible indicators for granite rheology: Contributions to Mineralogy and Petrology, v. 153, p. 121–138, doi: 10.1007/s00410-006-0142-z.

Zartman, R.E., 1964, A geochronologic study of the Lone Grove pluton from the Llano Uplift, Texas: Journal of Petrology, v. 5, p. 359–408.

Zartman, R.E., 1965, The isotopic composition of lead in microclines from the Llano Uplift, Texas: Journal of Geophysical Research, v. 70, p. 965–975, doi: 10.1029/JZ070i004p00965.

Manuscript Received 9 April 2008
Revised Manuscript Received 10 February 2009
Manuscript Accepted 10 February 2009

Printed in the USA